

Modeling the effects of graded and abrupt mole fraction profiles in pBn and nBn HgCdTe barrier detectors

*Original*

Modeling the effects of graded and abrupt mole fraction profiles in pBn and nBn HgCdTe barrier detectors / Alasio, Matteo; Vallone, Marco; Molino, Paolo; Errico, Luca; Hanna, Stefan; Figgemeier, Heinrich; Tibaldi, Alberto; Bertazzi, Francesco; Ghione, Giovanni; Goano, Michele. - ELETTRONICO. - 12687:(2023), pp. 1-5. ( SPIE Optical Engineering + Applications San Diego (USA) 20 - 24 August 2023) [10.1117/12.2682206].

*Availability:*

This version is available at: 11583/2983004 since: 2023-10-13T15:14:24Z

*Publisher:*

SPIE

*Published*

DOI:10.1117/12.2682206

*Terms of use:*

This article is made available under terms and conditions as specified in the corresponding bibliographic description in the repository

*Publisher copyright*

SPIE postprint/Author's Accepted Manuscript e/o postprint versione editoriale/Version of Record con

Copyright 2023 Society of PhotoOptical Instrumentation Engineers (SPIE). One print or electronic copy may be made for personal use only. Systematic reproduction and distribution, duplication of any material in this publication for a fee or for commercial purposes, and modification of the contents of the publication are prohibited.

(Article begins on next page)

# PROCEEDINGS OF SPIE

[SPIDigitalLibrary.org/conference-proceedings-of-spie](https://spiedigitallibrary.org/conference-proceedings-of-spie)

## Modeling the effects of graded and abrupt mole fraction profiles in pBn and nBn HgCdTe barrier detectors

Matteo Alasio, Marco Vallone, Paolo Molino, Luca Errico, Stefan Hanna, et al.

Matteo Alasio, Marco Vallone, Paolo Molino, Luca Errico, Stefan Hanna, Heinrich Figgemeier, Alberto Tibaldi, Francesco Bertazzi, Giovanni Ghione, Michele Goano, "Modeling the effects of graded and abrupt mole fraction profiles in pBn and nBn HgCdTe barrier detectors," Proc. SPIE 12687, Infrared Sensors, Devices, and Applications XIII, 126870E (10 October 2023); doi: 10.1117/12.2682206

**SPIE.**

Event: SPIE Optical Engineering + Applications, 2023, San Diego, California, United States

# Modeling the effects of graded and abrupt mole fraction profiles in pBn and nBn HgCdTe barrier detectors

Matteo G. C. Alasio<sup>1</sup>, Marco Vallone<sup>1</sup>, Paolo Molino<sup>1</sup>, Luca Errico<sup>1</sup>, Stefan Hanna<sup>3</sup>, Heinrich Figgemeier<sup>3</sup>, Alberto Tibaldi<sup>1,2</sup>, Francesco Bertazzi<sup>1,2</sup>, Giovanni Ghione<sup>1</sup>, and Michele Goano<sup>1,2</sup>

<sup>1</sup>Dipartimento di Elettronica e Telecomunicazioni, Politecnico di Torino, corso Duca degli Abruzzi 24, 10129 Torino, Italy

<sup>2</sup>IEIIT-CNR, corso Duca degli Abruzzi 24, 10129 Torino, Italy

<sup>3</sup>AIM Infrarot-Module GmbH, Theresienstraße 2, 74072 Heilbronn, Germany

## ABSTRACT

We present a numerical simulation study at 200 K of *pBn* and *nBn*  $\text{Hg}_{1-x}\text{Cd}_x\text{Te}$  barrier detectors, focused on the effects of the composition profile on the  $J$ - $V$  characteristics in dark. Considering a conventional barrier detector structure with three regions (absorber, barrier, cap), we discuss how the  $J$ - $V$  characteristics are affected by the steepness of the cap/barrier and barrier/absorber interfaces, especially in the nBn configuration.

**Keywords:** Infrared Detector, Barrier Detector, HgCdTe, graded HgCdTe composition profile

## 1. INTRODUCTION

Mercury cadmium telluride ( $\text{Hg}_{1-x}\text{Cd}_x\text{Te}$ ) is a ternary alloy semiconductor with electrical and optical properties suited for the entire spectrum of infrared (IR) applications.  $\text{Hg}_{1-x}\text{Cd}_x\text{Te}$  is one of the most employed semiconductors in a wide variety of IR devices, such as photodetectors, photoconductors, and complex structures like focal plane arrays (FPAs) for imaging.<sup>1-6</sup> Those applications are possible thanks to  $\text{Hg}_{1-x}\text{Cd}_x\text{Te}$  properties as its bandgap tunability and optical parameters that enable the fabrication of graded mole fraction profiles and high quantum efficiency devices.<sup>7,8</sup>

Conventional  $\text{Hg}_{1-x}\text{Cd}_x\text{Te}$  detectors require cryogenic temperatures for IR detection to reduce the dark current density,  $J_{\text{dark}}$ , to acceptable values. The main contributions to the dark current are Auger recombination (an intrinsic mechanism) and Shockley-Read-Hall recombination (SRH, an extrinsic mechanism dependent on the defect density).<sup>9-12</sup>

Recently, new devices such as barrier detectors have been designed to reduce the dark current associated with SRH recombination in depleted regions without blocking the photocurrents.<sup>13</sup> Therefore,  $\text{Hg}_{1-x}\text{Cd}_x\text{Te}$  barrier detectors have emerged as a possible solution to minimize dark current with negligible Auger generation-recombination and reduced impact of SRH.<sup>14</sup> Moreover,  $\text{Hg}_{1-x}\text{Cd}_x\text{Te}$  barrier detectors can operate at higher temperatures with respect to traditional detectors, thus overcoming the need of cryogenic temperatures.

In this work, we investigate the effects on the current-voltage  $J$ - $V$  characteristics in dark of graded profiles at the barrier interface with the absorber and the cap layers for both *nBn* and *pBn*  $\text{Hg}_{1-x}\text{Cd}_x\text{Te}$  barrier detectors. The simulated detectors feature a linearly graded interface across the barrier layer. We compare their  $J$ - $V$  characteristics against the one of an ideally abrupt composition profile.

---

Further author information: (Send correspondence to Matteo Alasio)

M. Alasio.: E-mail: matteo.alasio@polito.it

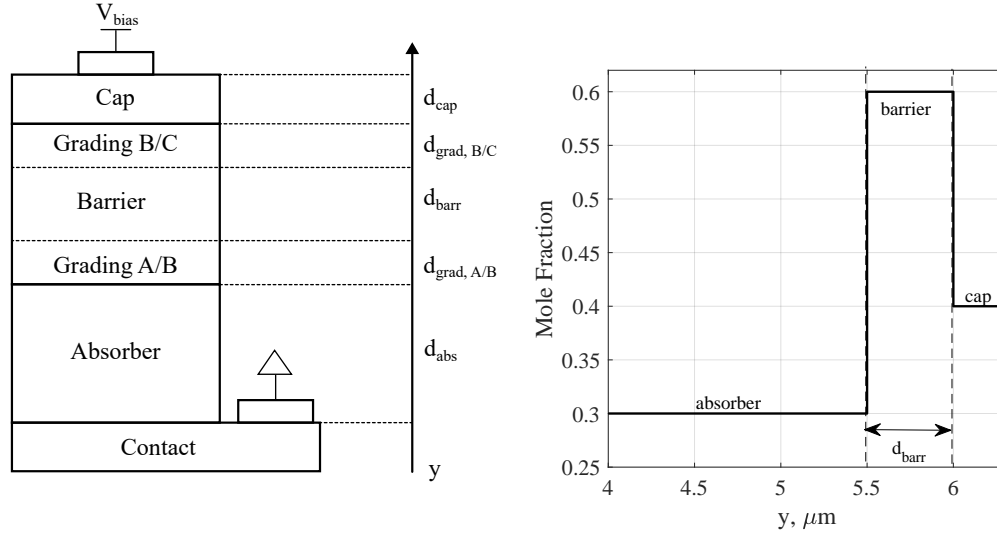


Figure 1. (Left) Cross-section of the detector with the relevant geometrical quantities. (Right) Abrupt  $pBn$  mole fraction composition profile for absorber, barrier, and cap layers.

## 2. GEOMETRY AND MODELING

The geometry of the barrier detector we studied consists of three layers, i.e., absorber, barrier, and cap, as illustrated in Fig. 1 (left).

The relevant quantities used in the geometry are summarized in Table 1. The absorber layer, with a thickness of  $d_{\text{abs}} = 5 \mu\text{m}$ , presents a constant mole fraction profile of  $x = 0.3$ . The barrier has a thickness  $d_{\text{barr}} = 0.5 \mu\text{m}$  and a mole fraction of  $x = 0.6$ . The cap layer mole fractions is  $x = 0.4$  in the  $pBn$  case and  $x = 0.3$  in the  $nBn$  configuration. In Fig. 1 (right), the mole fraction composition profile across the barrier layer is shown for the  $pBn$  abrupt configuration. In the study, the extension of the graded profile between absorber and barrier (A/B,  $d_{\text{grad,A/B}}$ ) and between barrier and cap (B/C,  $d_{\text{grad,B/C}}$ ) determines the total barrier thickness, reducing  $d_{\text{barr}}$ .

The doping profile presents abrupt transitions between the different layers. The absorber is doped  $N_{\text{abs}} = 5 \times 10^{15} \text{cm}^{-3}$ , the barrier  $N_{\text{barr}} = 1 \times 10^{15} \text{cm}^{-3}$  for the  $pBn$  case and  $N_{\text{barr}} = 1 \times 10^{14} \text{cm}^{-3}$  for the  $nBn$  case, and the cap  $N_{\text{cap}} = 1 \times 10^{15} \text{cm}^{-3}$ . The absorber is  $n$ -doped in both configurations, while the barrier, as well as the cap layer, is  $p$ -doped for the  $pBn$  case and  $n$ -doped for the  $nBn$  case. High  $n$ -doping concentration is present in the contact region of the absorber.

The numerical simulation framework is based on a quasi-1D model, and it implements drift-diffusion equations. The model includes Fermi statistics and incomplete ionization. SRH, radiative and Auger generation-recombination mechanisms are included in the simulation as they are the main mechanisms that dominate the dark current. All simulations use 200 K as a reference temperature.

Device	Layer	Dopant concentration	Geometrical Quantities		Mole Fraction
$pBn$	Absorber	$5 \times 10^{15} \text{cm}^{-3}$	$d_{\text{abs}}$	$5 \mu\text{m}$	0.3
	Barrier	$1 \times 10^{15} \text{cm}^{-3}$	$d_{\text{barr}}$	$0.5 \mu\text{m}$	0.6
	Cap	$1 \times 10^{15} \text{cm}^{-3}$	$d_{\text{cap}}$	$0.3 \mu\text{m}$	0.4
			$d_{\text{grad,A/B}}$	$0 \mu\text{m}$	
$nBn$	Absorber	$5 \times 10^{15} \text{cm}^{-3}$	$d_{\text{abs}}$	$5 \mu\text{m}$	0.3
	Barrier	$1 \times 10^{14} \text{cm}^{-3}$	$d_{\text{barr}}$	$0.5 \mu\text{m}$	0.6
	Cap	$1 \times 10^{15} \text{cm}^{-3}$	$d_{\text{cap}}$	$0.3 \mu\text{m}$	0.3
			$d_{\text{grad,A/B}}$	$0.2 \mu\text{m}$	

Table 1. Comparison of  $pBn$  and  $nBn$  configurations with their respective doping profiles, geometrical quantities, mole fractions, and extensions of the graded regions at the absorber/barrier interface ( $d_{\text{grad,A/B}}$ ).

### 3. RESULTS AND DISCUSSION

This Section presents and discusses the results obtained from our numerical investigation on the  $pBn$  and  $nBn$  configurations. The aim is to identify how graded mole fraction profiles impact the equilibrium band diagram, the  $J$ - $V$  characteristics, and the SRH rate.

First, Fig. 2 shows the equilibrium band diagrams of the  $pBn$  and the  $nBn$  configurations. The  $pBn$  configuration exhibits a valence band offset between the absorber and the barrier of approximately 45 meV, while the  $nBn$  configuration shows a valence band offset close to 80 meV. The  $pBn$  configuration has most of the barrier falling in the conduction band, thanks to the  $p$ -doped barrier profile. On the contrary,  $nBn$  configuration presents an almost un-doped barrier to minimize the equilibrium valence band offset. These differences influence the  $J$ - $V$  characteristic, particularly at lower biases. The effect in the  $J$ - $V$  characteristics can be seen in Fig. 3 and Fig. 4 in the  $[0, -0.2]$  V bias range.

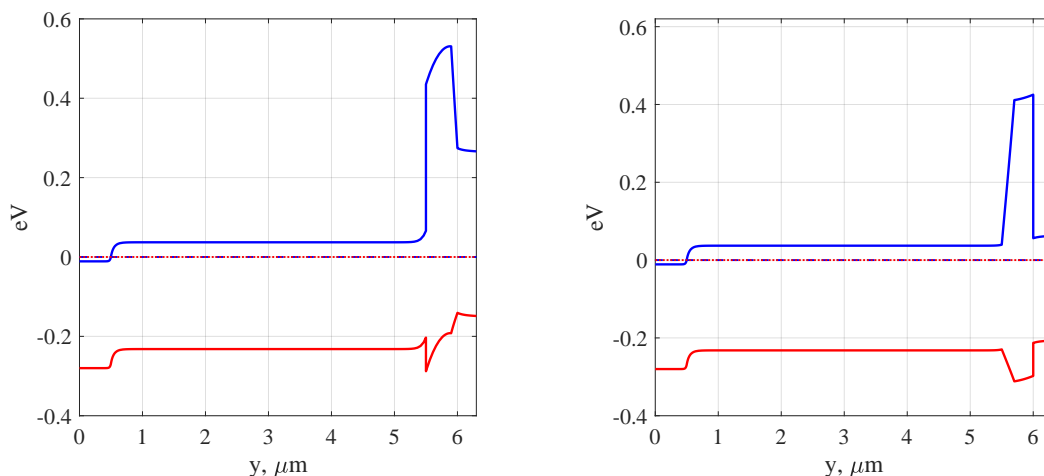


Figure 2. Equilibrium band diagram for the  $pBn$  (left) and  $nBn$  (right) configurations.

Fig. 3 reports the  $pBn$   $J$ - $V$  characteristic and compares the total and SRH recombination rates in the cap layer at the peak value. A dark current plateau determined by the hole current density is present in the reverse bias range of 0.1 up to 1 V for  $d_{\text{grad,B/C}} = 0$  nm. When increasing  $d_{\text{grad,B/C}}$  to 200 nm, the bias range corresponding to the dark current plateau shrinks from 0.1 to 0.5 V. The variation in the total current is due to the increase in the electron current density. The same increase is present in the SRH recombination rate. The reduction of the reverse bias range is compatible with the shift of the SRH generation mechanism as the  $d_{\text{grad,B/C}}$  is reduced. SRH is, in fact, the main generation mechanism and coincides with the total generation rate. For  $d_{\text{grad,B/C}} = 0$  nm, the SRH generation exceeds  $1 \times 10^{16} \text{ cm}^{-3}\text{s}^{-1}$  above 1 V reverse bias. For  $d_{\text{grad,B/C}} = 100$  nm and  $d_{\text{grad,B/C}} = 200$  nm, the generation exceeds  $1 \times 10^{16} \text{ cm}^{-3}\text{s}^{-1}$  above 0.7 V and 0.6 V reverse bias respectively. All the considered generation rates, as well as the current density, tend to saturate for high reverse bias applied.

Fig. 4 reports the  $nBn$   $J$ - $V$  characteristic and the total and SRH generation-recombination profiles, as with the  $pBn$  configuration. In this  $nBn$  configuration, only the case with an abrupt transition between the barrier and the cap shows a dark current plateau. The other grading profiles allow the flow of electron current density that prevents the intended behavior of the devices. When  $d_{\text{grad,B/C}} = 0$  nm, no SRH generation is present, and the total recombination rate is equal to the SRH recombination.

In conclusion, numerical simulations on barrier detectors show the sensitivity of  $J$ - $V$  characteristics with respect to the linear and abrupt composition profile. The  $nBn$  configuration has the most pronounced sensitivity to the grading profile, and only the abrupt configuration has the intended behavior. The  $pBn$  configurations are

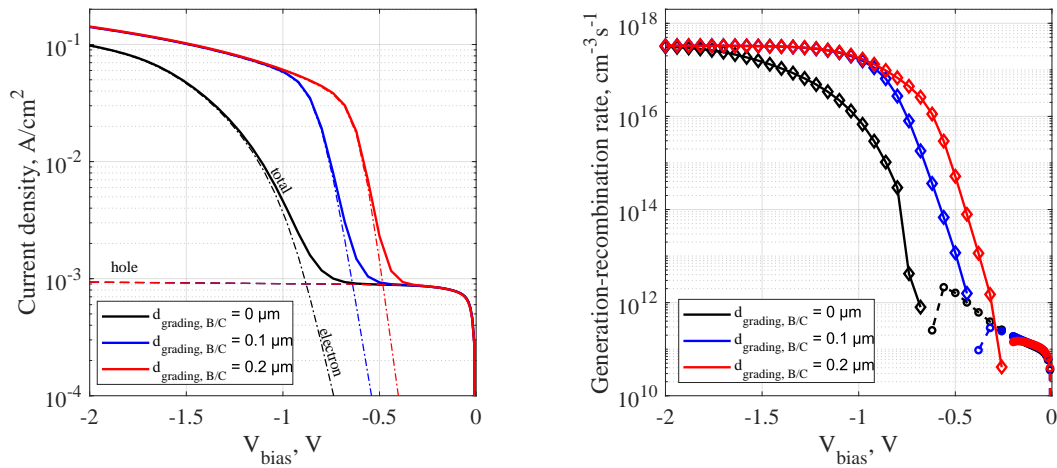


Figure 3.  $pBn$  configuration with different  $d_{\text{grad,B/C}}$  values.  $J$ - $V$  characteristics (left) and SRH and total generation-recombination rates within the cap layer at  $y = 6.15\mu\text{m}$  as a function of the applied bias (right). In the  $J$ - $V$  curves, the hole current is indicated by a dashed line, the electron current by a dotted line, and the total current by a solid line. In the SRH plot, SRH recombination is indicated by a dashed line, SRH generation by a solid line, total recombination by circular markers, and total generation by diamond markers.

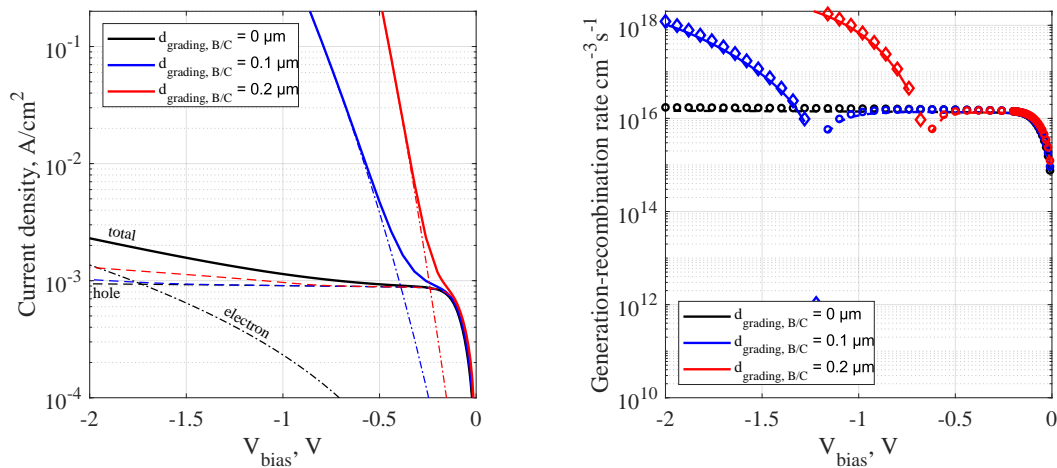


Figure 4.  $nBn$  configuration with different  $d_{\text{grad,B/C}}$  values.  $J$ - $V$  characteristics (left) and SRH and total generation-recombination rates within the cap layer at  $y = 6.15\mu\text{m}$  as a function of the applied bias (right). In the  $J$ - $V$  curves, the hole current is indicated by a dashed line, the electron current by a dotted line, and the total current by a solid line. In the SRH plot, SRH recombination is indicated by a dashed line, SRH generation by a solid line, total recombination by circular markers, and total generation by diamond markers.

less sensitive to the different grading profiles, but the shrink of the dark current plateau allows only a reduced set of applied biases. The simulations suggest possible graded mole fraction profile optimization of  $\text{Hg}_{1-x}\text{Cd}_x\text{Te}$  barrier detectors, with the potential of enhancing the efficacy of barrier detectors by controlling dark current and minimizing SRH effects.

## REFERENCES

- [1] Rogalski, A., Antoszewski, J., and Faraone, L., “Third-generation infrared photodetector arrays,” *J. Appl. Phys.* **105**(9), 091101 (2009).
- [2] Kinch, M. A., “HgCdTe: Recent trends in the ultimate IR semiconductor,” *J. Electron. Mater.* **39**(7), 1043–1052 (2010).
- [3] Martyniuk, P., Antoszewski, J., Martyniuk, M., Faraone, L., and Rogalski, A., “New concepts in infrared photodetector designs,” *Appl. Phys. Rev.* **1**, 041102 (2014).
- [4] Gravrand, O., Rothman, J., Cervera, C., Baier, N., Lobre, C., Zanatta, J. P., Boulade, O., Moreau, V., and Fieque, B., “HgCdTe detectors for space and science imaging: general issues and latest achievements,” *J. Electron. Mater.* **45**(9), 4532–4541 (2016).
- [5] Rogalski, A., Martyniuk, P., Kopytko, M., and Hu, W., “Trends in performance limits of the HOT infrared photodetectors,” *MDPI Appl. Sci.* **11**(2), 501 (2021).
- [6] Lei, W., Antoszewski, J., and Faraone, L., “Progress, challenges, and opportunities for HgCdTe infrared materials and detectors,” *Appl. Phys. Rev.* **2**(4), 041303 (2015).
- [7] Rogalski, A., “HgCdTe infrared detector material: history, status and outlook,” *Rep. Prog. Phys.* **68**, 2265–2336 (2005).
- [8] Kinch, M. A., Aqariden, F., Chandra, D., Liao, P.-K., Schaake, H. F., and Shih, H. D., “Minority carrier lifetime in *p*-HgCdTe,” *J. Electron. Mater.* **34**(6), 880–884 (2005).
- [9] Kopytko, M., Józwiowski, K., Martyniuk, P., and Rogalski, A., “Photon recycling effect in small pixel p-i-n HgCdTe long wavelength infrared photodiodes,” *Infrared Phys. Technol.* **97**, 38–42 (2019).
- [10] Lee, D., Dreiske, P., Ellsworth, J., Cottier, R., Chen, A., Tallaricao, S., Yulius, A., Carmody, M., Piquette, E., Zandian, M., and Douglas, S., “Law 19: The ultimate photodiode performance metric,” in [*Infrared Technology and Applications XLVI*], **11407, Proceedings of the SPIE**, 114070X, SPIE (2020).
- [11] Kopytko, M. and Rogalski, A., “New insights into the ultimate performance of hgcdte photodiodes,” *Sens. Actuators A* **339**, 113511 (2022).
- [12] Zhu, M., Prighozhin, I., Mitra, P., Scritchfield, R., Schaake, C., Martin, J., Park, J. H., Aqariden, F., and Bellotti, E., “Dark current and gain modeling of mid-wave and short-wave infrared compositionally graded hgcdte avalanche photodiodes,” *IEEE Trans. Electron Devices* **69**(9), 4962–4969 (2022).
- [13] Martyniuk, P., Gawron, W., and Rogalski, A., “Theoretical modeling of HOT HgCdTe barrier detectors for the mid-wave infrared range,” *J. Electron. Mater.* **42**, 3309–3319 (2013).
- [14] Martyniuk, P., Kopytko, M., and Rogalski, A., “Barrier infrared detectors,” *Opto-Electron. Rev.* **22**(2), 127–146 (2014).